Tetragonal high-pressure phase of ZnO predicted from first principles

Zhenwei Li, Ying Xu, Guoying Gao, Tian Cui, and Yanming Ma*
State Key Laboratory of Superhard Materials, Jilin University, Changchun 130012, People's Republic of China
(Received 18 December 2008; revised manuscript received 8 April 2009; published 6 May 2009)

We report a high-pressure tetragonal PbO-type structure ($B10$) of ZnO predicted through *ab initio* lattice-dynamics calculation. This structure can be directly transformed from NaCl structure ($B1$) along an orthorhombic $Pmmn$ transition path and can be viewed as alternatively stacked layers of cations and anions with the anion layer composed of zigzag arranged anionic rows. Enthalpy curve calculation suggests that $B10$ is stable in a large pressure range of 236–316 GPa, above which CsCl structure ($B2$) takes over. Band-structure calculation reveals that this polymorph is a wide band-gap semiconductor with an energy gap larger than 2.95 eV.

DOI: 10.1103/PhysRevB.79.193201 PACS number(s): 64.70.K−, 61.50.Ks, 62.50.−p, 63.20.D−

Zinc-oxide (ZnO) semiconductor is one of the most intriguing materials with a variety of technological applications, such as transparent field-effect transistors, light-emitting diodes, ultraviolet nanolasers, photodetectors, solar cells, catalysis, and chemical sensors.[1–3] Also, ZnO exists naturally as a mineral and its high-pressure phase is of great geological importance as a component of the lower mantle.[4] The electronic and structural properties of ZnO have thus been a renewing topic in the research community over the last 60 years.

ZnO crystallizes at ambient conditions in the wurtzite structure ($P6_3mc$, $Z=2$, and $B4$), which is a typical form in the *IIB-VIA* and *IIIA-VA* binary compounds. Under compression a transition to the NaCl phase ($Fm\text{-}3m$, $Z=1$, and $B1$) at ~10 GPa was well established both experimentally and theoretically.[5–12] The origin of this transition has been suggested to be the softening of the shear elastic modes (C_{44} and C_{66}) of $B4$ phase.[10,13] With regard to higher pressures, however, there is only an empirical yet widely accepted hypothesis on the $B1 \rightarrow B2$ transition in analogy to the alkali halides and alkaline-earth oxides.[14] Liu *et al.*[12] made an experimental attempt to detect the transition but no transformation sign up to their highest pressure of 209 GPa. Theoretically, Jaffe *et al.*[15] predicted the $B1 \rightarrow B2$ transition at 256 and 260 GPa from first-principles study within generalized gradient approximation (GGA) and local-density approximation (LDA), respectively, while atomistic calculation done by Zaoui and Sekkal[13] determined the transition at 305 GPa. Recently, Amrani *et al.*[16] reported a transition pressure of 243.5 GPa using the full-potential linearized augmented plane wave method. Although these calculations have been carried out to probe the high-pressure transition of ZnO, they were limited by the static calculation of $B2$ structure, which may miss some unexpected yet more stable phases. Phonons are believed to load more subtle information on the structural stability and to be a powerful tool to probe the transition mechanisms.[17–20] Therefore a lattice-dynamics investigation is extensively performed to explore the high-pressure structure of ZnO. Indeed, a tetragonal high-pressure structure ($P4/nmm$) was uncovered and found to be stable in a large pressure range of 236–316 GPa, above which $B2$ structure takes over.

Our phonon calculations were performed using the density functional theory (DFT) (Refs. 21 and 22) and the linear-response perturbation theory[23,24] as implemented in the QUANTUM-ESPREESO package.[25] GGA exchange-correlation functional of Perdew, Burke, and Ernzerhof (PBE) (Refs. 26 and 27) is used, and norm-conserving pseudopotentials are generated within the scheme suggested by Troullier and Martins[28] with valence-electron configurations of $Zn: 3d^{10}4s^2$ and $O: 2s^2 2p^4$. Kinetic-energy cutoff of 180 Ry and Monkhorst-Pack (MP) k meshes of $8\times8\times8$ and $6\times6\times9$ for the cubic and tetragonal structures, respectively, are employed to ensure the total energy convergence within ~1 meV/atom. MP $4\times4\times4$ and $3\times3\times5$ q meshes are used in the interpolation of phonon bands for the cubic and tetragonal phases, respectively.

Figure 1(a) compares the calculated P-V curves for $B1$ phase with experimental data.[7,12] Excellent agreement is seen

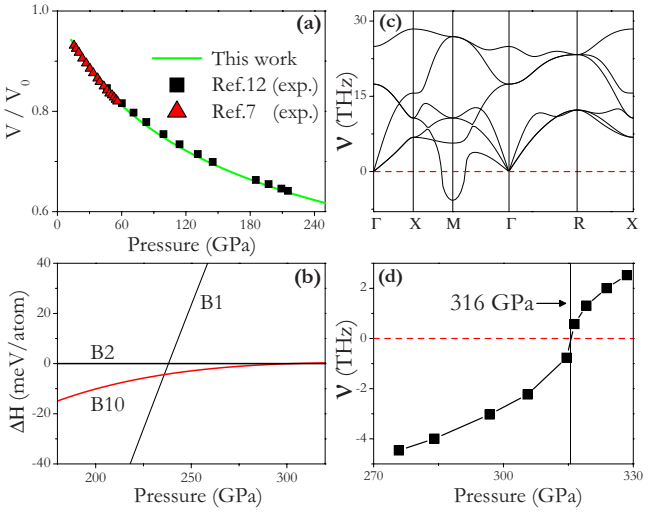

FIG. 1. (Color online) (a) The calculated P-V relation for $B1$ phase together with experimental data from Desgreniers (Ref. 7) and Liu *et al.* (Ref. 12). The theoretical P-V curve is derived by fitting the calculated volume vs energy data into the Murnaghan equation of sate. (b) Enthalpy of $B1$ and $B10$ relative to that of $B2$. The $B10$ phase is more stable than $B1$ above 236 GPa and converges with $B2$ above 316 GPa. (c) Phonon dispersion curves of $B2$ at 250 GPa. (d) Evolution of the TA(M) phonon frequency with increasing pressures. The vertical solid line marks the critical pressure above which $B2$ becomes dynamically stable.

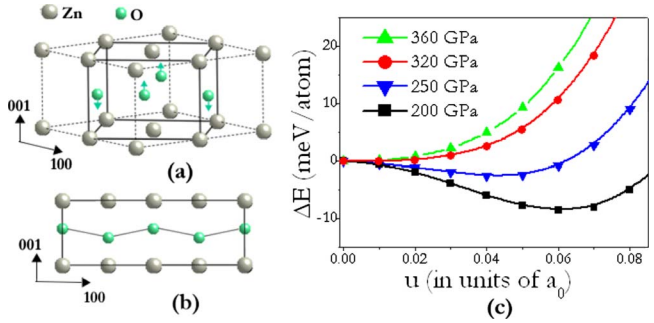

FIG. 2. (Color online) (a) The dashed unit cell is a $2\times2\times1$ supercell of $B2$ structure. Oxygen (small sphere) atomic distortion along the eigenvector of TA(M) mode as indicated by the arrows results in the formation of $B10$ phase (solid unit cell). (b) Top view of the $B10$ structure along the [010] direction. (c) Energy evolution curves with the oxygen displacements along the eigenvector of TA(M) mode at 200, 250, 320, and 360 GPa, respectively. The total energies are normalized to that of $B2$ for comparison.

throughout the wide high-pressure range, supporting the current methods and pseudopotentials adopted. Transition from $B1$ to $B2$ takes place at 238 GPa as suggested by our enthalpy calculation [Fig. 1(b)] under the static condition of equal enthalpies. This value is somewhat lower than those by Jaffe *et al.*[15] and Zaoui and Sekkal[13] but in good consistency with that by Amrani *et al.*[16] As a whole, they are all in line with the experimental observation that $B1$ remains stable up to the pressure as high as 200 GPa.[12] Our calculated phonon bands for $B2$ phase at 250 GPa are plotted in Fig. 1(c) where severely softened transverse acoustic (TA) phonons appear at the M point (0.5,0.5,0.0), indicating the structural instability of $B2$ at this pressure. Evolution of the TA(M) phonon frequency with increasing pressures reveals that $B2$ can be stabilized only above 316 GPa [Fig. 1(d)]. Clearly, the direct $B1\rightarrow B2$ transition is not realistic and an intermediate phase is calling for assignment. Our effort below is thus devoted to identifying this phase by adopting a method of freezing phonon.[19]

A phonon frequency is the second-order derivative of the total energy with respect to a vibration eigenvector (denoted as VR); therefore, an imaginary phonon ($\nu^2<0$) corresponds to the saddle point in the multidimensional energy surface and atomic displacement along the VR should lead to the true energy minimum. This can be expressed by the following simplified equation: $\Delta E=(1/2)m\nu^2\Delta u^2$, where E is the static total energy, ν is the phonon frequency, u is the displacement along the VR, and Δ indicates the corresponding small variation of E and u. For VR of the TA(M) mode, zinc atoms stay relatively static while oxygen atoms in the body center of two adjacent $B2$ cells move oppositely along the c axis of the crystal [Fig. 2(a)]. Energy evolution curves in Fig. 2(c) are thus derived from distortions along this VR at the selected pressures. It is evident that at higher pressures (e.g., 320 and 360 GPa), $B2$ structure is stable. However, at lower pressures of 200 and 250 GPa, the energy minima lie in the distortion path and, therefore, a lower-energy structure is formed [Fig. 2(a)].

The predicted structure often referred to as $B10$ has a tetragonal lattice with space group of $P4/nmm$. At 250 GPa,

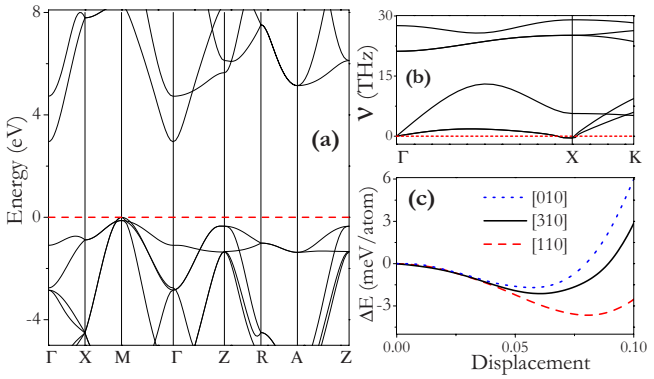

FIG. 3. (Color online) (a) Energy band structure of $B10$ at 250 GPa. (b) Phonon dispersion curves of $B1$ along the Γ-X-K direction at 250 GPa. (c) Energy evolution curves with respect to the shearing displacements of (001) planes in $B1$ at 290 GPa along three different directions of [010], [310], and [110]. The distorted structures along the three directions have the space groups of $Cmcm$, $P2_1/m$, and $Pmmn$, respectively. Displacements have been scaled to the lattice parameter a_0 of $B1$. Note that energy curves with other displacement directions lie in between [010] and [110] with all of the distorted structures having space group of $P2_1/m$.

its optimized lattice parameters are $a=3.237$ Å and $c/a=0.71$, with zinc and oxygen atoms occupying $2a$ (0, 0, 0) and $2c$ (0, 1/2, 0.4531), respectively. This structure can be viewed as alternatively stacked anionic and cationic layers. While its cationic layer is the same planar structure as $B2$, its anionic layer is puckered into zigzag arranged anionic rows which make it distinguished from $B2$ [Fig. 2(b)]. With this $B10$ phase in hand, a transition sequence of $B1\rightarrow B10\rightarrow B2$ is revealed by comparison of their enthalpies [Fig. 1(b)]. It is found that $B10$ is thermodynamically stable in the pressure range of 236–316 GPa, above which it transforms to the $B2$ phase with a typical second-order transition nature. We have calculated the full phonon dispersion curves of $B10$, and no any imaginary phonon mode was found in the whole Brillouin zone (BZ) to confirm its dynamical stability.

To understand the $B1\rightarrow B10$ transition mechanism, we have further explored the dynamical stability of $B1$ phase and a pressure-driven TA phonon softening is clearly revealed at the X point [Fig. 3(b)]. The two degenerated TA(X) modes (perpendicular to each other) involve antiparallel shuffle of adjacent (001) planes of $B1$. It is suggested that this mode degeneracy enables the shuffle movements bringing forth any shear distortion perpendicular to the c axis. Figure 3(c) shows the energy evolution curves with different shear distortions. It is found that the lowest-energy structure is formed when the distortion is along the [110] direction. Strikingly, optimization of this distorted-$B1$ structure [space group: $Pmmn$; $Z=2$; and Wyckoff positions: Zn at $2a$ (0, 0, $z1$) and O at $2b$ (1/2, 0, $z2$)] at 290 GPa arrives at the $B10$ phase. This nicely demonstrates that the reconstructive $B1\rightarrow B10$ transition is driven by the softening of TA(X) phonon and can be accomplished along an intermediate orthorhombic $Pmmn$ path. The $Pmmn$ structure reduces to $B1$ when $b=c=a/\sqrt{2}$, $z1=z2=0.75$ and transforms to $B10$ when $a=b$, $z1=0.5$, and $z2=0.97$ (e.g., at 290 GPa). The $B1\rightarrow B10$ transition is thus characterized by enlarging of b

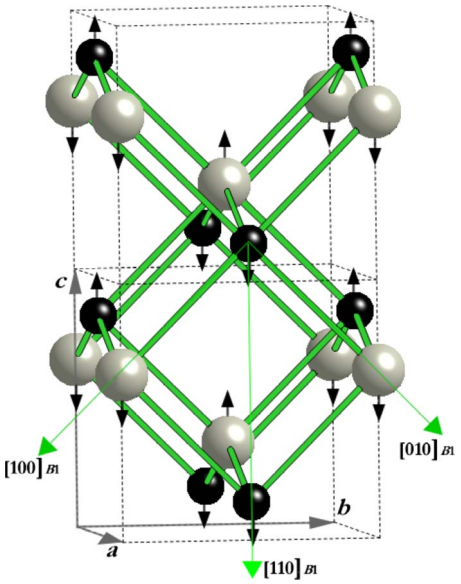

FIG. 4. (Color online) Schematic representation of the $B1 \rightarrow B10$ transformation in a $1 \times 1 \times 2$ supercell of *Pmmn* structure. Lattice parameters *a*, *b*, and *c* of the *Pmmn* structure are labeled, and the [100], [010], and [110] crystal directions of the pristine *B*1 structure are also shown for comparison. The *B*10 and *Pmmn* structures share the same crystal orientation. The antiparallel shuffle movement (indicated by arrows) of adjacent (001) planes of *B*1 along the $[110]_{B1}$ direction causes the zinc (large gray sphere) and oxygen (small black sphere) ions to detach from each other along the *c* axis and results in the formation of *B*10 structure with separated cation and anion layers.

and the splitting of $z1$ and $z2$. A schematic description of this transition is depicted in Fig. 4. It is clearly seen that the splitting of $z1$ and $z2$ actually corresponds to the shuffle movement of adjacent layers in *B*1 along the $[110]_{B1}$ direction and signals the detachment of the anions and cations from the same plane to form alternatively arranged anion layer and cation layer which are typical characteristics of *B*10 structure. It is noteworthy that the enlarged *b* at the transition might be closely related to the strong Coulomb repulsion within the anion or cation layer. It should be also pointed out that the predicted TA(X) mode softening in ZnO is in line with the results in other binary compounds with *B*1 structure.[29–31] However, the resulting higher-pressure phase of *B*10 in ZnO is distinct, in contrast to that of *Cmcm* (Ref. 29) in ZnS, ZnSe, InP, and InAs and $P2_1/m$ (Ref. 31) in AgBr and AgCl. This can be explained by the different shuffle directions favorable in these materials. If the shear distortion favors the [010] direction, *Cmcm* phase will be most stable.[29] Instead, if the true energy minimum lies in distortion path along other directions between [010] and [110], this will result in a lower-symmetry $P2_1/m$ phase.[31]

Energy band structure of *B*10 at 250 GPa is shown in Fig. 3(a). It is clear that this polymorph remains insulating with a large indirect band gap of 2.95 eV. It is well known that DFT usually underestimates the energy gap by about 30 %–50 %, the actual band gap in *B*10 should be much larger. *GW* calculation[32] (known to provide accurate description of band gaps, within 10% of the experimental values) is necessary to fully account for the energy gap, but is out of scope of this work. The large band gap implies that the *B*10 phase is of great potential in the electronic and optic applications as what we are expecting for the high-pressure *B*1 and *B*2 phases.[33,34] Future experiments to quench or synthesize this polymorph at ambient conditions are thus demanded.

In conclusion, we have predicted a *B*10 phase in ZnO sitting in between *B*1 and *B*2. This finding modifies earlier long thought of the direct $B1 \rightarrow B2$ high-pressure transition. The stability of *B*10 is justified by the enthalpy calculations, and its dynamical stability has been confirmed by the phonon calculations. The phase transition mechanism of $B1 \rightarrow B10$ is revealed by analysis of TA(X) phonon softening in *B*1, and an orthorhombic transition path with *Pmmn* symmetry is accordingly proposed. The current work has demonstrated that phonons play a dominant role in determining the high-pressure structures.

We are thankful for financial support from the China 973 Program under Grant No. 2005CB724400, the National Natural Science Foundation of China under Grant No. 10874054, the NSAF of China under Grant No. 10676011, and the 2007 Cheung Kong Scholars Programme of China.

*Author to whom correspondence should be addressed; mym@jlu.edu.cn

[1] K. Nomura, H. Ohta, K. Ueda, T. Kamiya, M. Hirano, and H. Hosono, Science **300**, 1269 (2003).
[2] C. T. Lee, Y. K. Su, and H. M. Wang, Thin Solid Films **150**, 283 (1987).
[3] M. H. Huang, S. Mao, H. Feick, H. Yan, Y. Wu, H. Kind, E. Weber, R. Russo, and P. Yang, Science **292**, 1897 (2001).
[4] L. Liu, *High-Pressure Research, Applications in Geophysics* (Academic, New York, 1977).
[5] F. J. Manjón, K. Syassen, and R. Lauck, High Press. Res. **22**, 299 (2002).
[6] S. C. Yu, I. L. Spain, and E. F. Skelton, Solid State Commun. **25**, 49 (1978).
[7] S. Desgreniers, Phys. Rev. B **58**, 14102 (1998).
[8] J. M. Recio, M. A. Blanco, V. Luaña, R. Pandey, L. Gerward, and J. S. Olsen, Phys. Rev. B **58**, 8949 (1998).
[9] H. Karzel, W. Potzel, M. Köfferlein, W. Schiessl, M. Steiner, U. Hiller, G. M. Kalvius, D. W. Mitchell, T. P. Das, P. Blaha, K. Schwarz, and M. P. Pasternak, Phys. Rev. B **53**, 11425 (1996).
[10] F. Decremps, J. Zhang, B. Li, and R. C. Liebermann, Phys. Rev. B **63**, 224105 (2001).
[11] L. Gerward and J. J. S. Olsen, J. Synchrotron Radiat. **2**, 233 (1995).
[12] H. Liu, J. S. Tse, and H.-K. Mao, J. Appl. Phys. **100**, 093509 (2006).
[13] A. Zaoui and W. Sekkal, Phys. Rev. B **66**, 174106 (2002).
[14] Ü. Özgür, Y. I. Alivov, C. Liu, A. Teke, M. A. Reshchikov, S.

Doğan, V. Avrutin, S.-J. Cho, and H. Morkoç, J. Appl. Phys. **98**, 041301 (2005).
[15] J. E. Jaffe, J. A. Snyder, Z. Lin, and A. C. Hess, Phys. Rev. B **62**, 1660 (2000).
[16] B. Amrani, I. Chiboub, S. Hiadsi, T. Benmessabih, and N. Hamdadou, Solid State Commun. **137**, 395 (2006).
[17] Y. Ma, J. S. Tse, and D. D. Klug, Phys. Rev. B **67**, 140301(R) (2003).
[18] Y. Li, L. J. Zhang, T. Cui, Y. W. Li, Y. M. Ma, Z. He, and G. T. Zou, J. Phys.: Condens. Matter **19**, 425217 (2007).
[19] Y. Li, Y. Ma, Y. Yan, T. Cui, and G. Zou, Appl. Phys. Lett. **92**, 101907 (2008).
[20] Y. Ma, J. S. Tse, and D. D. Klug, Phys. Rev. B **69**, 064102 (2004).
[21] P. Hohenberg and W. Kohn, Phys. Rev. **136**, B864 (1964).
[22] W. Kohn and L. J. Sham, Phys. Rev. **140**, A1133 (1965).
[23] P. Giannozzi, S. deGironcoli, P. Pavone, and S. Baroni, Phys. Rev. B **43**, 7231 (1991).
[24] S. Baroni, P. Giannozzi, and A. Testa, Phys. Rev. Lett. **58**, 1861 (1987).
[25] S. Baroni, S. de Gironcoli, A. Dal Corso, and P. Giannozzi, http://www.pwscf.org/.
[26] J. P. Perdew, K. Burke, and M. Ernzerhof, Phys. Rev. Lett. **77**, 3865 (1996).
[27] J. P. Perdew and K. Burke, Int. J. Quantum Chem. **57**, 309 (1996).
[28] N. Troullier and J. L. Martins, Phys. Rev. B **43**, 1993 (1991).
[29] V. Ozolinš and A. Zunger, Phys. Rev. Lett. **82**, 767 (1999).
[30] J. Zhang, L. Zhang, T. Cui, Y. Li, Z. He, Y. Ma, and G. Zou, Phys. Rev. B **75**, 104115 (2007).
[31] Y. Li, L. Zhang, T. Cui, Y. Ma, G. Zou, and D. D. Klug, Phys. Rev. B **74**, 054102 (2006).
[32] M. Shishkin and G. Kresse, Phys. Rev. B **75**, 235102 (2007).
[33] J. E. Jaffe, R. Pandey, and A. B. Kunz, Phys. Rev. B **43**, 14030 (1991).
[34] J. Sun, H.-T. Wang, J. He, and Y. Tian, Phys. Rev. B **71**, 125132 (2005).